MNRAS **000**, 1–10 (2015) Preprint 17 December 2020 Compiled using MNRAS LATEX style file v3.0

# Injection of magnetic helicity in solar cycle 24 from the observations of magnetic fields

H. Zhang[1]★, S. Yang[1], K. Kuzanyan[1,2], A. Brandenburg[3,4], H. Xu[1], & D. Sokoloff[2,5]

[1] *National Astronomical Observatories, Chinese Academy of Sciences, Beijing 100012, China,*
[2] *IZMIRAN, Russian Academy of Sciences, Troitsk, Moscow 142190, Russia*
[3] *Nordita, KTH Royal Institute of Technology and Stockholm University, Roslagstullsbacken 23, SE-10691 Stockholm, Sweden*
[4] *Department of Astronomy, AlbaNova University Center, Stockholm University, SE-10691 Stockholm, Sweden*
[5] *Department of Physics, Moscow University, 119992 Moscow, Russia*

Accepted XXX. Received YYY; in original form ZZZ

## ABSTRACT

The injection of magnetic helicity with solar cycle 24th has been calculate based on the analysis of a series of magnetic synoptic charts. During the cycle, the injective magnetic helicity is mainly contributed by the magnetic field in active regions. It is hard to find the helicity near the polar regions due to the eruption of the helicity into the interplanetary space from the solar surface. The mean values of the injective magnetic helicity flux is consistent with the hemispheric sign rule of current helicity of solar active regions, i.e. the negative (positive) sign tends to be in the northern (southern) hemisphere. Significant fluctuations of the injected magnetic helicity from the subsurface layers probably reflect the complex process of how the twist from the convection zone ejects magnetic fields through a series of active regions on different temporal and spatial scales at the solar surface.

**Key words:** Sun – Photosphere – Magnetic field

## 1 INTRODUCTION

Helicity is an important quantity that reflects the topology of the field, such as linkage, twist, and writhe of the field lines (Woltjer 1958a,b; Taylor 1986). It is an integral measure of the topological properties of the field in a closed volume $V$:

$$H_f = \int \mathbf{F} \cdot \nabla \times \mathbf{F} dV, \quad (1)$$

where $\mathbf{F}$ can be the magnetic vector potential $\mathbf{A}$, the magnetic field $\mathbf{B}$, or the velocity field $\mathbf{V}$, which is assumed to be confined to the volume $V$.

In the solar atmosphere, the magnetic and velocity fields are observable quantities with vector magnetographs, while the magnetic potential $\mathbf{A}$ and the electric current density $\mathbf{J}$ $(= \nabla \times \mathbf{B}/\mu_0)$ are derived quantities under some assumptions (cf. Zhang 2000, 2019; Zhang *et al.* 2003). The computation of helicity in the Sun requires the knowledge of the full vector field in a 3D volume, but observations of the magnetic fields are usually taken in a shallow layer of the solar atmosphere (typically, in the photosphere). Due to the limitation of the observations of vector magnetic fields in a single layer of the solar atmosphere, it is difficult to construct the real distribution of all components of the current density in the solar photosphere (Xu et al. 2015). This means that we still cannot get all components of the current density, not even in the lower solar photosphere. The similar case is also for the magnetic potential $\mathbf{A}$. This means that the completeness of the helicity has been lost from the calculations by means of the observations of vector magnetograms.

Nevertheless, the magnetic helicity density $h_{\rm m} = \mathbf{A} \cdot \nabla \times \mathbf{A}$, current helicity density $h_c = \mathbf{B} \cdot \nabla \times \mathbf{B}$, and velocity helicity density $h_v = \mathbf{V} \cdot \nabla \times \mathbf{V}$ are still important detectable quantities. For example, one can calculate a part of the current helicity density $h_c = 3(\mathbf{B})_z \cdot (\nabla \times \mathbf{B})_z$ inferred from observed photospheric vector magnetograms under the isotropic assumption (Xu et al. 2015) and the injection rate of magnetic helicity from the solar subsurface regions (Chae 2001) based on the photospheric magnetograms. This implies that the analysis of helicities involves observable quantities in the solar atmosphere only. In addition, it is normally believed that the complex distribution of magnetic (current) helicity density in the solar active regions relates with the trigger of powerful flares and CMEs (cf. Bao *et al.* 1999; Liu & Zhang 2006; Zhang et al. 2008).

The helical topology of magnetic fields in active re-

★ E-mail: hzhang@bao.ac.cn

gions was firstly observed from the handedness of sunspot penumbral configurations by Hale et al. (1908) and statistically with respect to hemispheres by Ding et al. (1987). The hemispheric sign rule of helicity was subsequently analyzed by Seehafer (1990), who found that the current helicity density and twist in solar active regions follows the hemispheric helicity rule with predominantly negative values in the northern hemisphere and positive values in the southern hemisphere. It is noted that a violation of the magnetic helicity sign rule in the beginning of each solar cycle was discovered by Bao et al. (2000) based on observations of a series of vector magnetograms at Huairou Solar Observing Station and a reversal of the helicity sign rule with time by Hagino & Sakurai (2005) from the observations at National Astronomical Observatory of Japan. The distribution of current helicity of active regions in solar cycles 22 and 23 was presented by Zhang et al. (2010), the injection of magnetic helicity by Yang & Zhang (2012) and Zhang & Yang (2013), and also the magnetic helicity by Pipin et al. (2019) for solar cycle 24 based on the vector field synoptic maps.

The importance of the magnetic helicity for the solar dynamo has been noticed (cf. Pouquet et al. 1975; Kleeorin & Ruzmaikin 1982; Brandenburg & Subramanian 2005) after the development of the solar dynamo theory with the turbulence of velocity field in the solar convection zone (i.e., the early stage of the mean field dynamos). By means of a flux transport dynamo model, Choudhuri et al. (2004) explained that the hemispheric helicity could reverse sign at the beginning of each cycle, as seen in the observations of Bao et al. (2000). A similar work has been proposed based on the analytical solution of the mean field dynamo model by Xu et al. (2009), who found that a reversed sign of mean hemispheric helicity can also occur in the decaying stage of a cycle. While the more complex distribution of magnetic helicity with the solar cycle can be found from the butterfly diagrams of mean current helicity of solar active regions in solar cycles 22 and 23 (Zhang et al. 2010), and also confirmed from the injection of global magnetic helicity from the solar surface by Yang & Zhang (2012) and Zhang & Yang (2013).

Section 2 presents the injection of magnetic helicity during solar cycle 24 inferred by the large-scale magnetic fields. Section 3 describes the magnetic helicity and the relationship with evolution of magnetic field in the individual active regions. Section 4 discusses our findings.

## 2 INJECTION OF MAGNETIC HELICITY IN SOLAR CYCLE 24

It is generally believed that the magnetic fields and the corresponding helicity in the solar surface are important parameters to understanding possible effects on the solar dynamo process in the solar convection zone where the $\alpha$ effect is one of the key parameters in this process (e.g. Parker 1955; Steenbeck et al. 1966; Zeldovich et al. 1983). The magnetic (current) helicity is an important ingredient in the $\alpha$ effect; see Brandenburg & Subramanian (2005) for a review.

The collective effect of the active regions on the contribution of magnetic (current) helicity with the solar cycle has been studied from observations (such as Zhang et al. 2010; Yang et al. 2012; Zhang, Brandenburg and Sokoloff 2016) and also with solar dynamo models (see, e.g., Kleeorin et al. 2003; Choudhuri et al. 2004; Xu et al. 2009; Pipin et al. 2013, for example).

In the following, we study the injection of magnetic helicity during solar cycle 24, using the method of Yang & Zhang (2012) and Zhang & Yang (2013). We also study the distribution of the magnetic helicity flux in the butterfly diagram.

### 2.1 Method

The transfer of magnetic helicity is accompanied with the dynamo process within the Sun. Corresponding discussions have been provided by Kleeorin & Ruzmaikin (1982) and Kleeorin et al. (1995). The variation of the mean value of the fluctuating small-scale magnetic helicity, $h_{\rm m} = \langle \mathbf{a}\cdot\mathbf{b}\rangle$, can be written in the form

$$\frac{\partial h_{\rm m}}{\partial t} = -2\langle(\mathbf{u}\times\mathbf{b})\cdot\mathbf{B}\rangle - 2\eta_m\langle(\mathbf{b}\cdot(\nabla\times\mathbf{b})\rangle - \langle(\nabla\cdot[\mathbf{a}\times(\mathbf{u}\times\mathbf{b})]\rangle, \tag{2}$$

where $\mathbf{b}$, $\mathbf{u}$, and $\mathbf{B}$ are the fluctuating magnetic field, the fluctuating velocity field, and the mean magnetic field, respectively. The effective electromotive force $\mathbf{E_{eff}} \equiv \langle(\mathbf{u}\times\mathbf{b})\rangle = \alpha\mathbf{B} - \eta(\nabla\times\mathbf{B})$ is give by Moffatt (1978); Parker (1979); Zeldovich et al. (1983); Brandenburg & Subramanian (2005), so equation (2) becomes

$$\frac{\partial h_{\rm m}}{\partial t} = 2[\eta\mathbf{B}\cdot(\nabla\times\mathbf{B}) - \alpha\mathbf{B}^2 - \eta\langle(\mathbf{b}\cdot(\nabla\times\mathbf{b})\rangle] - \nabla\cdot\mathbf{F}_{\rm hel}, \tag{3}$$

where $\alpha = \alpha_v + \alpha_{\rm m}$ and $\eta = \eta_{\rm m} + \eta_T$. The integrals of the magnetic helicity in the northern and southern hemispheres are, even if the total magnetic helicity is normally conserved, can be written

$$\frac{dH_{\rm m}}{\partial t} = \int_V 2[\eta\mathbf{B}\cdot(\nabla\times\mathbf{B}) - \alpha\mathbf{B}^2 - \eta\langle(\mathbf{b}\cdot(\nabla\times\mathbf{b})\rangle]dv - \oiint_S \mathbf{F}_{\rm hel}\cdot d\mathbf{s}, \tag{4}$$

where the helicity flux $\mathbf{F}_{\rm hel} = \langle\mathbf{a}\cdot\mathbf{b}\rangle\mathbf{V} - \langle(\mathbf{V}\cdot\mathbf{a})\mathbf{b}\rangle + \langle\mathbf{a}\times\mathbf{u}\rangle\times\mathbf{B} + \langle\mathbf{a}\times(\mathbf{u}\times\mathbf{b})\rangle\cdots$, and $\mathbf{a}$ is the fluctuating magnetic potential and $\mathbf{V}$ is the mean velocity field (Kleeorin & Rogachevskii 1999; Brandenburg & Subramanian 2005). The first term in the right-hand side of equation (4) relates to the generation of magnetic helicity field inside the domain $V$ (such as the Sun) and the second to the injection of helicity flux from the surface $S$ in the exterior of the solar dynamo.

The injective magnetic helicity from the surface containing twist or linkage of magnetic fields can be written in the form (Berger & Field 1984; Demoulin & Berger 2003)

$$F_{\rm m} = \frac{dH_{\rm m}}{dt} = \frac{d}{dt}\int_V h_{\rm m}\,dv = -2\oiint_S[(\mathbf{V}_t\cdot\mathbf{A}_p)\mathbf{B}_n - (\mathbf{A}_p\cdot\mathbf{B}_t)\mathbf{V}_n]\cdot d\mathbf{s}, \tag{5}$$

where the magnetic field $\mathbf{B}$ and the velocity field $\mathbf{V}$ are observed quantities in the solar atmosphere, and the boundary value of the magnetic vector potential $\mathbf{A}_p$ of the potential of the reference field reference field can be inferred from the vertical component of the magnetic field $B_n$.

where the magnetic field **B** and the velocity field **V** are observed quantities in the solar atmosphere, and the boundary value of the magnetic vector potential of the potential reference field, $\mathbf{A}_p$, can be inferred from the vertical component of the magnetic field $B_n$. The subscripts $n$ and $t$ indicate the normal and transverse component, respectively.

The first term in the right hand side of equation (5) provides the contribution from the horizontal motion of footpoints of magnetic field at the solar surface, while the second one reflects the contribution from the vertical motion of magnetic flux at the surfaces of the integral.

Both equations (3) and (5) have been used to analyze the evolution of magnetic helicity from different perspectives. The former equation has been used in the study of the magnetic helicity with the dynamo process, and latter on the injective flux of magnetic helicity from the enveloping surface, such as the solar surface. Agreement between the two methods can be taken as an indication of the validity of the analysis concerning the evolution of large-scale magnetic fields over the solar cycle.

The three components of the velocity field in the photosphere can also be derived from the Differential Affine Velocity Estimator for Vector Magnetograms (DAVE4VM; Schuck 2008). As one neglects the second term in the right hand side of equation (5), there is an error of about 10% in the calculation of the injected magnetic helicity as compared with the method DAVE4VM, as pointed out by Liu & Schuck (2012) from their calculated results.

According to the analysis of Demoulin & Berger (2003), one finds that

$$\frac{dH_{\rm m}}{dt} = -2 \oiint_S (\mathbf{U} \cdot \mathbf{A}_p)\mathbf{B}_n \cdot d\mathbf{s}, \tag{6}$$

where

$$\mathbf{U} = \mathbf{V}_t - \frac{V_n}{B_n}\mathbf{B}_t .$$

This implies that the influence of the second term in equation (5) has been neglected because only the line of sight magnetograms have been used. It has been used in our following calculation, as the one ignores the influence of some errors discussed above.

It is noticed that equation (6) with the local correlation tracking (LCT) method (Chae 2001) for calculating the horizontal velocity field of magnetic features has been used to analyze the large-scale injective magnetic helicity at the solar surface of cycle 23 by means of MDI magnetic synoptic charts (Yang & Zhang 2012) and the MDI 96min full-disk magnetograms (Zhang & Yang 2013). It also shows the similar tendency on the large-scale reversal of the sign distributions of magnetic helicity with solar cycles in the northern and southern hemispheres as compared with the calculation of the mean current helicity of active regions by Zhang et al. (2010).

In the following, we study the injective helicity in solar cycle 24 and its possible latitudinal distribution with time.

### 2.2 Distribution of injective magnetic helicity in solar cycle 24

In this study, 122 HMI magnetic synoptic charts in the period between 2010-June-02 and 2019-March-26 have been used in the calculation to obtain the longitudinal butterfly diagrams in Fig. 1a. It includes the most part of the magnetic fields in solar cycle 24. It is noticed that most of the magnetic field migrates toward the equator, and also some to the polar regions (Wang et al. 1989) along the meridional flow in the solar convection zone (Zhao et al. 2013).

For analyzing the transfer of the magnetic helicity contributed from the magnetic fields, Fig. 1b shows the butterfly diagram of mean injective magnetic helicity inferred by a seres of HMI synoptic charts by means of equation (6). It shows the mean values of injective helicity with the latitude at various solar Carrington rotation cycles. This result reflects the contribution of large temporal and spatial scale magnetic fields to the magnetic helicity in the magnetic synoptic charts. This means that the results reflected in Figs 1a and 1b show similar temporal and spatial scales.

It is pointed out by Zhang, Brandenburg and Sokoloff (2016) that around the solar maximum the magnetic energy and helicity spectra are steeper, emphasizing the large-scale field. This tendency can also be found in Fig. 1, where the large-scale structures are the result of smaller elements of magnetic field and helicity of the same sign tend during the maximum of the solar cycle.

From Fig. 1, it is found that the injected magnetic helicity at the solar surface shows a trace to the equator with the migration of the large scale magnetic field and also shows a tendency toward the northern and southern poles, but it is hard to find the helicity in the polar regions. It reflects that most of the helicity has been erupted with the evolution of magnetic fields of active regions and cannot reach the solar polar regions. Figure 1b shows the injected magnetic helicity with the variation of magnetic features corresponding to temporal and spatial scales calculated from a series of synoptic magnetic charts.

Figure 1c shows the smoothed injective helicity with solar cycle 24 for displaying the mean contribution of magnetic helicity. It is easy to see that the relatively strong large-scale positive injective helicity patterns occur near Carrington rotation (CR) 2155 in the southern hemisphere and that near CR 2175 in the northern hemisphere, and negative one occurs between CRs 2115 and 2135 in the northern hemisphere etc. It also needs to be emphasized that the accuracy of the calculation of the magnetic helicity in high latitudes is low due to the influence of projective effects on the observed magnetograms and the corresponding synoptic charts.

A similar pattern of the butterfly diagram of mean current helicity of active regions has been presented by Zhang et al. (2010) using the 6205 observed vector magnetograms of 984 solar active regions at Huairou Solar Observing Station (most of the large solar active regions in solar cycle 22 and 23 have been included). From a theoretical point of view, consistence between equations (5) and (3) can be found, because the variation of mean magnetic helicity density $\partial h_{\rm m}/\partial t$ in equation (3) relates to the current helicity and also the $\alpha$ factor of the solar dynamo statistically. This means that the transfer of magnetic helicity (twisted magnetic flux loops) brings the current helicity from the subsurface to the solar surface, and the latter can be detectable from the photospheric vector magnetograms. The correlation between the change of magnetic and current helicity in individual solar active regions has been discussed by Liu & Zhang (2006) and Zhang et al. (2008).

Figure 2 shows the mean injective rate of magnetic he-

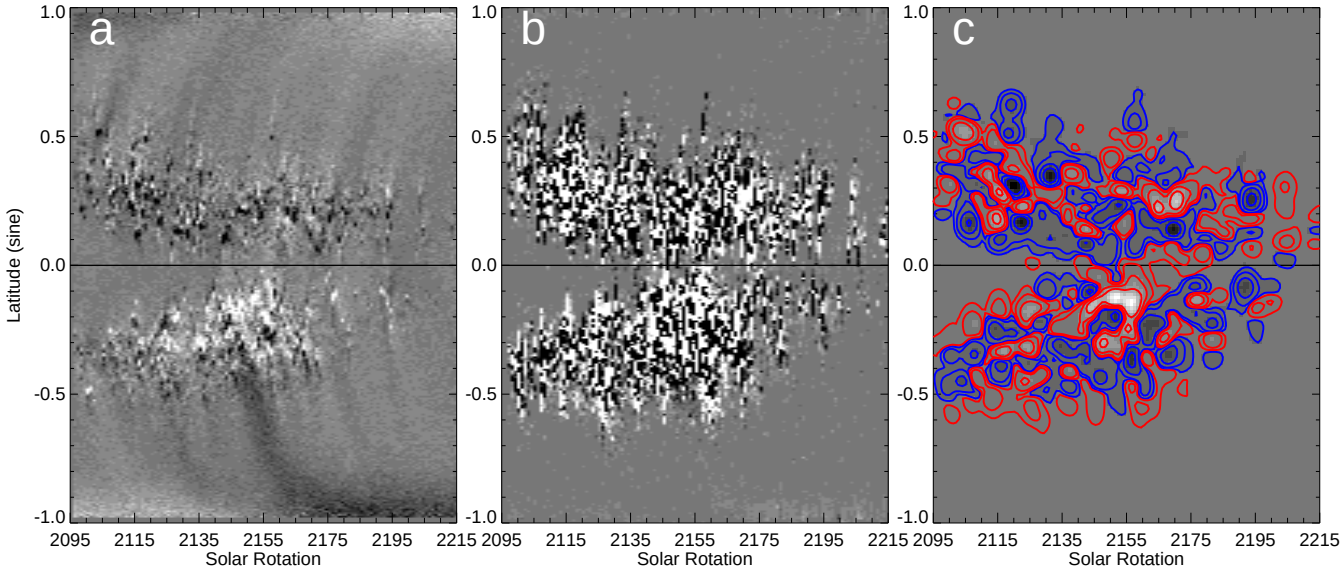


**Figure 1.** a) Butterfly diagram of magnetic fields in solar cycle 24th. The white (black) in positive (negative) polarity. b) The distribution of the injective rate of magnetic helicity in the both hemispheres. The white (black) shows positive (negative) sign. c) The injective rate of magnetic helicity in the both hemispheres after the smooth. The red (blue) contours show the relative injective rates of 1, 5, 20, 50 $\times 10^{32}(\mathrm{Mx})^2/s$ in the positive (negative) signs.

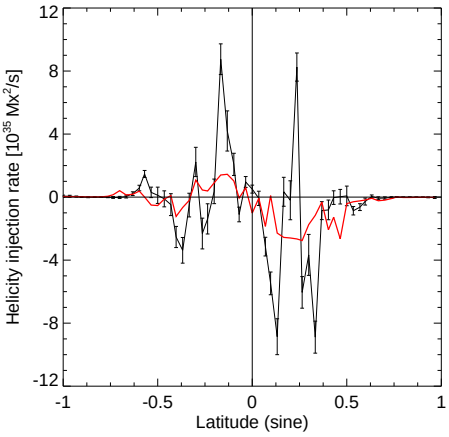


**Figure 2.** The mean injective rate of magnetic helicity with the latitude in solar cycle 24th. The error bars show the relative deviation of the mean values only. The red line marks the distribution of injective magnetic helicity after the smooth.

licity with latitude. It is found that the dominant sign is negative in the northern hemisphere and positive in the southern hemisphere. This tendency can also be found from the smoothed result in Fig. 1c. It is consistent with the hemispheric sign rule of magnetic helicity (Seehafer 1990) and also the result for the solar cycle 23 by Yang & Zhang (2012) and Zhang & Yang (2013), and for the solar cycle 24 by Pipin et al. (2019). Some slight difference relative to the results of Pipin et al. (2019) for solar cycle 24 is probably caused by the use of different methods. The result of Pipin et al. (2019) provide additional magnetic (current) helicity in the solar atmosphere.

Figure 3 shows the mean injective rate of magnetic helicity in the northern and southern hemispheres with solar cycle 24 based on the calculation of a series of HMI synoptic magnetic charts. The mean values in the northern and southern hemispheres are $-83.7\,\mathrm{Mx}^2,\mathrm{s}^{-1}$ and $66.6\,\mathrm{Mx}^2\,\mathrm{s}^{-1}$, respectively. It provides a rough estimation on the distribution of the injective magnetic helicity in the solar atmosphere. The total flux of injective magnetic helicity flux in this calculation is on the order of $10^{44}\mathrm{Mx}^2$ in the whole solar cycle 24, while it is lower than $5\times10^{46}\,\mathrm{Mx}^2$, as estimated by Zhang & Yang (2013), because this calculation is based on the magnetic synoptic charts, some short temporal and spatial magnetic flux and its contribution for the helicity flux have been ignored.

The difference on the estimation of the total magnetic helicity from the solar surface between that by Zhang & Yang (2013) with the MDI 96 minute full-disk magnetograms and our calculation with the magnetic synoptic charts is of the order of $5\times10^2$. The difference on the temporal intervals of the data series of the magnetic field for the calculation of the injected helicity by us and that by Zhang & Yang (2013) is a order of $4\times10^2$. This means that a certain mount of injected helicity has been lost in our calculation. This also means that the results of Zhang & Yang (2013) provide a lower estimate of the injective helicity from the solar surface during the solar cycles, because the contribution from short time scales of less than 96 minutes has been neglected.

Figure 4 shows the distribution of the mean magnetic field with longitude in the northern and southern hemispheres in solar cycle 24 and the corresponding injective rate of magnetic helicity inferred from the magnetic synoptic charts, which are contributed by the magnetic fields of a series of active regions. In Figs 4a and d, it is easy to see the slanted arrangement of a series of magnetic field structures like scratches in both hemispheres caused by the differential rotation of the Sun. One can also see a large-scale pattern of the injective helicity after the data are smoothed in Fig. 4c and 4f. It is consistent with the idea that the dominant sign

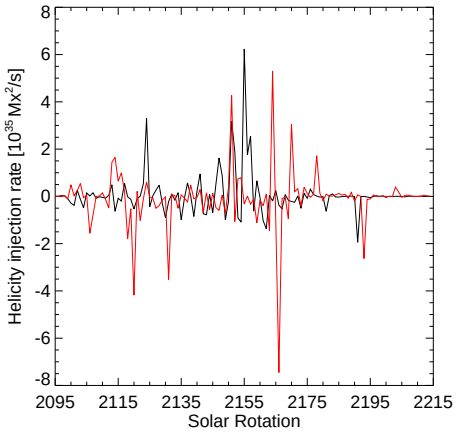


**Figure 3.** The injective rate of magnetic helicity in the northern (red) and southern (black) hemisphere along the latitude in solar cycle 24th.

of the injective helicity shows a negative sign in the northern hemisphere and a positive one in the southern hemisphere. It is also true of Fig. 1c and 2. The relatively strong large-scale negative injective helicity patterns occurs near CR 2135 in the northern hemisphere and positive ones near CR 2155 in the southern hemisphere. This is consistent with the result in Fig. 1c.

## 3 MAGNETIC HELICITY FROM INDIVIDUAL ACTIVE REGIONS

Although the injection of magnetic helicity in the solar atmosphere has been presented from photospheric vector magnetograms (such as Zhang 2001; Liu & Zhang 2006), the comparison between the averaged magnetic helicity and the individual contributions from active regions is also useful for understanding the contribution of magnetic helicity from the solar surface. To analyze the magnetic helicity in the lower solar atmosphere, we introduce a sample of active regions such as active region NOAA12673 and the subsequent relative active regions. Active region NOAA12673 was observed in September 2017 by the *Heliospheric Magnetic Imager* (HMI) and *Atmospheric Imaging Assembly* (AIA) on board the *Solar Dynamics Observatory* (SDO). This active region was a typical fast developing $\delta$ region with 4 X-class and 27 M-class flares during its passage across the visible solar disk (cf. Yang et al. 2017; Sun & Norton 2017; Romano et al. 2019).

The magnetic field in active region NOAA 12673 and the possible topology of overlapping magnetic lines of force in the top of view are shown in Fig. 5. The newly emerging magnetic flux is marked by red arrowed lines and the existing magnetic field by green ones. Comparing with the evolution of the large-scale magnetic field, it is found that the new magnetic flux emerges near the photospheric inversion line of the active region to form highly sheared magnetic field in the solar atmosphere. This probably reflects the interaction of two different systems of magnetic lines of force, i.e., the new reversed magnetic lines formed in the deeper layer of the sub-atmosphere occurred in the developed active region to reverse the distribution of the magnetic field in the photosphere from Hale's rule (Getling 2019). This probably means that the local evolution of the magnetic field at the solar surface is controlled by the magnetic field formed in different layers of the convection zone.

The statistical analysis of the emergence of magnetic flux with twisted magnetic loops from the subsurface was proposed by Longcope et al. (1998). Although it is favorable to compare with observations in both mean value and statistical dispersion, it is also very important to track the evolution process of magnetic flux with helicity in individual active regions.

Figure 6 shows a series of synoptic charts of the magnetic field at different CRs and the corresponding time difference. It provides an opportunity to analyze the large-scale magnetic fields for the detection of a possible evolution of magnetic fields from the subsurface. This is a sequence of solar active regions NOAA 12670, 12673, 12682, and 12685. It is found that the leading and following polarities of the large-scale magnetic bipoles change in time before and after the emergence of active region NOAA 12673. This provides evidence for a reversed variation of the observed large-scale magnetic bipole of active regions due to the emergence of negative magnetic helicity flux from the deeper solar convection zone. This is similar for the highly sheared magnetic field occurred in the active region NOAA12681 in the southern hemisphere with the injection of magnetic helicity.

Figure 6 also shows the injective rate $G = -(\mathbf{V}_t \cdot \mathbf{A}_p)B_n$ calculated from the synoptic magnetic charts and the corresponding horizontal velocity $\mathbf{V}_t$ by LCT after some smoothing. The horizontal velocity arrows due to the evolution of the large-scale magnetic fields in the solar surface are inferred from LCT. The consistency in the direction of the velocity field with the evolving direction of the large-scale magnetic fields can normally be found, for example in the active regions NOAA 12670, 12673, and 12682. It is also noticed that the contribution of the helicity in the quiet Sun is negligible.

It is found that a major contribution of the magnetic helicity $G = -(\mathbf{V}_t \cdot \mathbf{A}_p)B_n$ comes from the active regions, even if this only provides the variation of magnetic fields on the synoptic scale, while the relatively small temporal scale ones have been ignored. However, comparing with all solar cycles, it can also be presented as the contribution from the fluctuated magnetic fields. From the evolution of the large-scale magnetic fields in Fig. 6, we suggest that these reflect the local exchange between the poloidal and toroidal fields emerging from in the subsurface.

In Fig. 6 it is seen that the contribution of the horizontal velocity with the injective magnetic helicity occurs in local areas of active regions. This occupy only a relative small amount in the magnetic charts due to the smaller contribution from the quiet Sun.

Since we use the LCT method to obtain the horizontal velocity, there may be a loss of some magnetic helicity signal. Here we use the auto-correlation function to evaluate the lost. As an example, Fig. 7 shows the auto-correlation function for different latitudes along the time direction of CR 2193 in Fig. 6a. It is found that the auto-correlation function is much sharper at the region without sunspots. While using the LCT method, this may cause a low correlation and underestimates the movements at small scales. Thus, we obtain a relatively small amplitude of magnetic he-

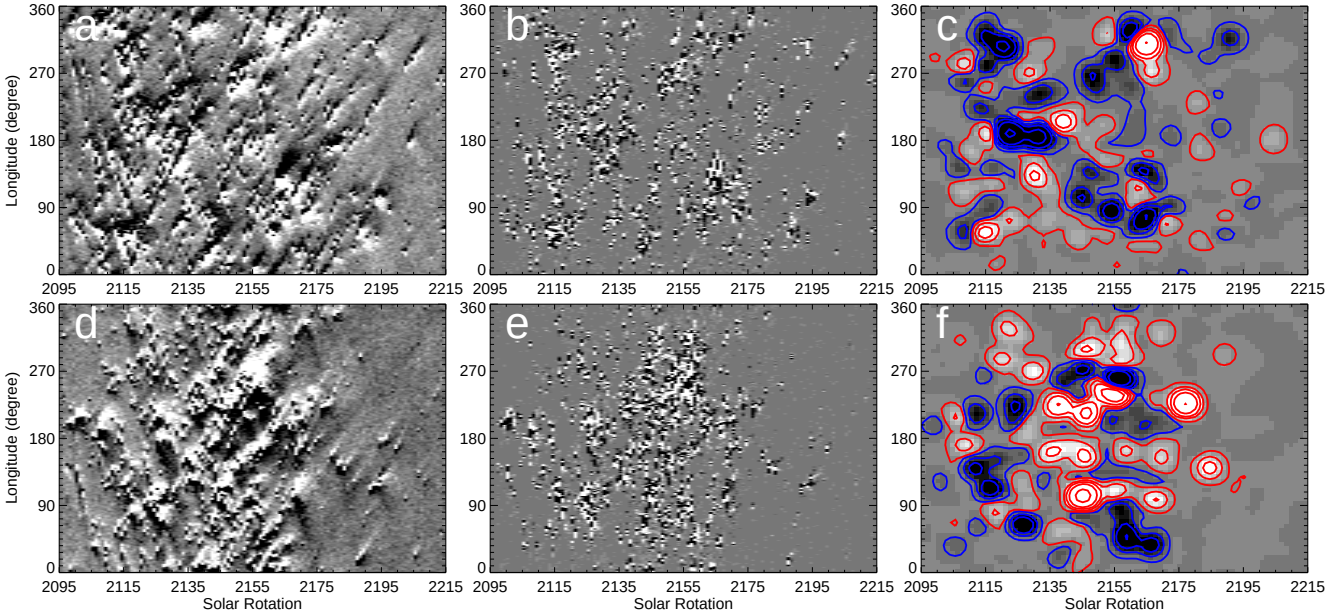


**Figure 4.** Left: mean magnetic field with the longitude in the northern (a) and southern (d) hemisphere in solar cycle 24. Middle: the corresponding injective rate of magnetic helicity in the both hemispheres (b and e). Right: injective rate of magnetic helicity in the both hemispheres (c and f) after smoothing. Red (blue) contours show the injective rates of 1, 5, 10, and $20\times10^{32}$ Mx$^2$ s$^{-1}$ in positive (negative) signs.

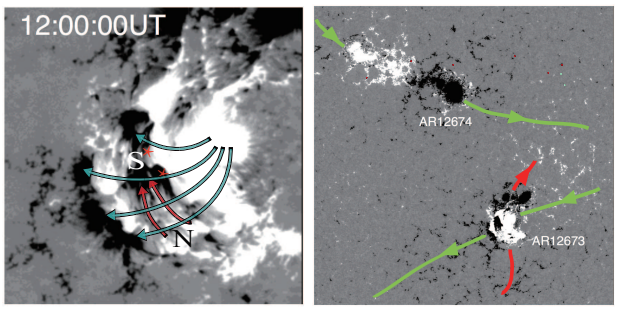


**Figure 5.** Left: The interaction between the existed magnetic fields in active region NOAA 12673 (the green line with arrow) and the reversely emerging magnetic flux (red one) from deep convection zone in the top of view on September 4, 2017. Size is $125'' \times 125''$. Right: The relationship between the magnetic field between active region NOAA 12673 and 12674 in the large scale field of view. Size is $750'' \times 750''$. The top is the north and left is east.

licity fluxes compared with previous results, such as those of Yang & Zhang (2012) and Zhang & Yang (2013). However, this could still reflect helicity flux characteristic at the specific spatial resolution and temporal cadence. This is also consistent with the local contribution of injective helicity from the large-scale field distributed in Fig. 6a.

## 4 EXPLANATION OF INJECTIVE MAGNETIC HELICITY WITH SOLAR CYCLES

As one follows the theoretical analysis of the solar dynamo and comparing with the observations, the magnetic field can be separated to the mean field component and fluctuation field one. The formal one relates to the mean field dynamo with large scale helicity (Kleeorin et al. 2003; Zhang et al. 2012), while second one to the fluctuated helicity, probably with some exchange of the signs of the helicity in the solar surface. The emergence of magnetic field brings the magnetic helicity from the solar convection zone into the solar surface. It is usually believed that in this process the total magnetic helicity tends to be conserved in the approximation of large Reynolds number, and the fluctuation contribution of the different scale magnetic helicity is neglected in many studies of the solar cycle.

It is noticed that the obvious fluctuations of injective helicity occurred at the surface comparing on solar cycle scales; see, for example, Figs 1b, 4b, 4e, and 6, as well as the findings by Zhang & Yang (2013). This reflects the generation of magnetic fields in the convection zone is a complex process, i.e., the helical magnetic field probably formed at the different layers in the deep solar convection zone and with different helical tendencies probably.

It is interesting that the amount of magnetic flux injected from the convection zone into the solar atmosphere during the solar cycle is provided by means of equation (6), and this is roughly compatible with the description of the second term $-\oiint_S \mathbf{F}_{\rm hel} \cdot d\mathbf{s}$ in the right-hand side of equation (5).

For analyzing the distribution of magnetic helicity with the cycle, the simplest case of a solar dynamo by Parker (1955) has been used to compare with the behavior of an $\alpha\omega$ dynamo wave near a given latitude $\theta$, and the equations

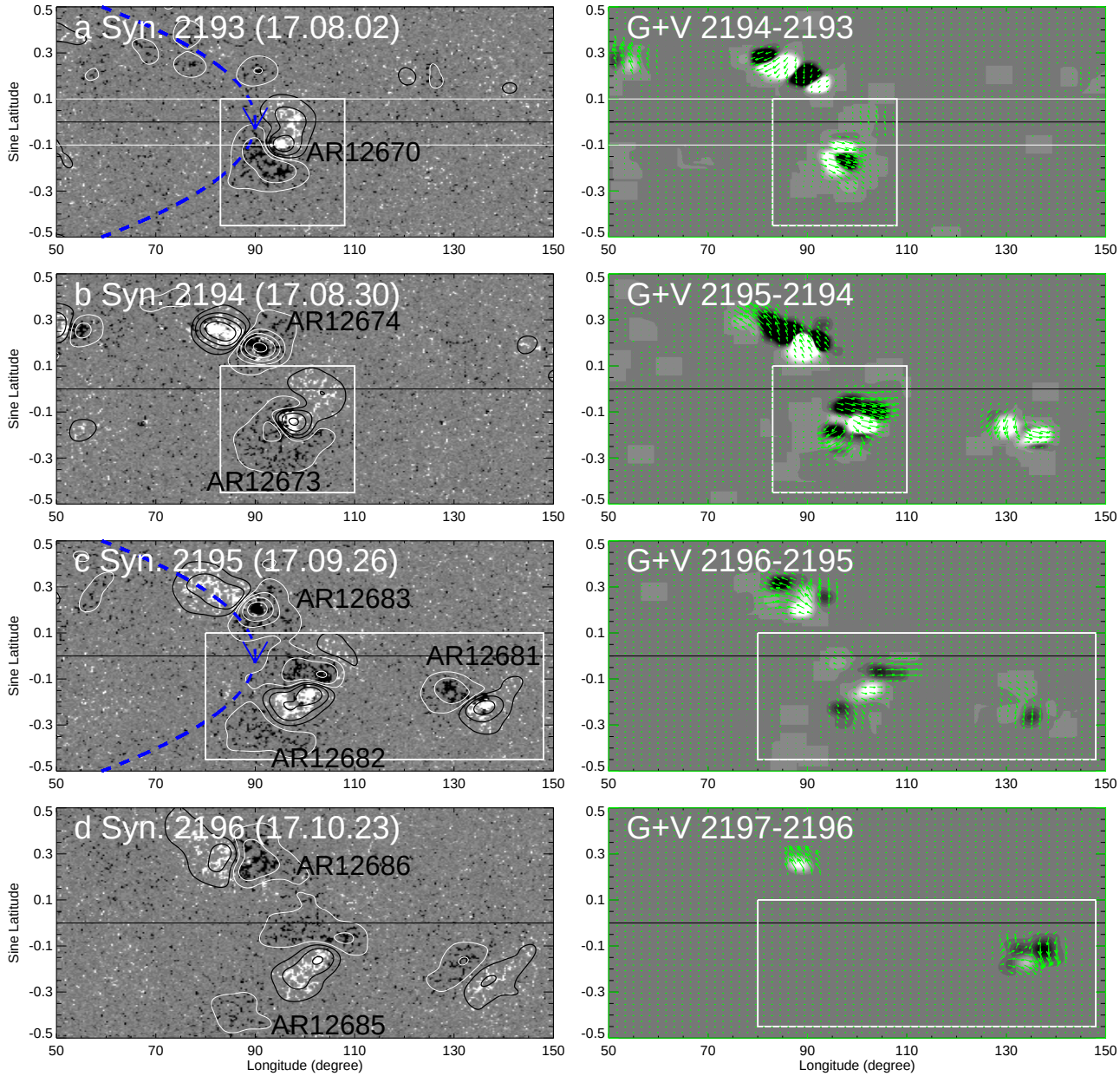


**Figure 6.** Left: Evolution of large scale magnetic fields of active region NOAA 12673 and the relationship with active regions NOAA 12670, 12682, and 12685 in the synoptic charts of different Carrington rotations 2193-2196. The blue dashed lines with arrows mark the regular direction of magnetic fields in the convection zone according to the Hale polarity low of magnetic fields. The contour levels (black/white) of the smoothed magnetic fields are ±5, 20, 50, 100, and 200 G. Right: Injective rate $G = -(\mathbf{V}_t \cdot \mathbf{A}_p)B_n$ (white (black) shows the positive (negative) sign), and the horizontal velocity (arrows) inferred by LCT.

assume the form (Kleeorin et al. 2003)

$$\frac{\partial B}{\partial t} + V\frac{\partial B}{\partial \theta} = D\frac{\partial A}{\partial \theta} + \lambda\frac{\partial^2 B}{\partial \theta^2},$$
$$\frac{\partial A}{\partial t} + V\frac{\partial A}{\partial \theta} = \alpha B + \lambda\frac{\partial^2 A}{\partial \theta^2}, \qquad (7)$$

where $V$ is the large-scale flow, $D$ is the dynamo number ($D \sim \Omega(\theta, r)$), where is the angular velocity and $r$ is in the direction of the solar radius) and $\lambda$ is the turbulent diffusivity. $D(\Omega)$ and $\alpha$ are topologically important parameters relative to the stretch and twist of the magnetic field in the solar dynamo model. The solar differential rotation is related to the quantity $D(\Omega)$. The spectral analysis of $\alpha$ effect has been presented in the theory of solar dynamo (such as Moffatt 1978; Parker 1979; Zeldovich et al. 1983; Brandenburg & Subramanian 2005). The contribution of the different typical scales of the velocity and magnetic fields is a notable question.

As one follows the Figs 1-6 and the variation of the magnetic field with the depth, we can assume the form of a traveling wave in equations (7) in the form of the Fourier

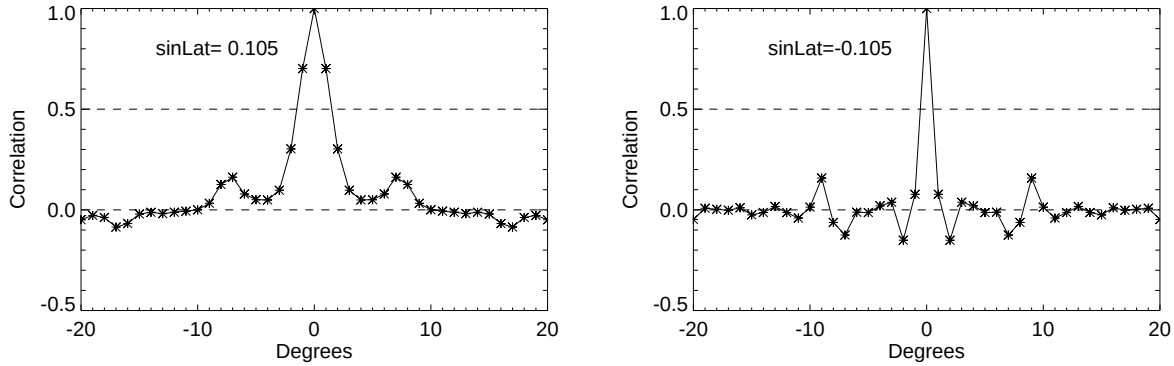


**Figure 7.** Auto correlation function distribution of the different latitude along the time direction of CR2193 (labeled by two straight white horizontal solid lines in the figure 6a.) Left: relative to active region, the low line and right: the quiet Sun, the top line in figure 6a.

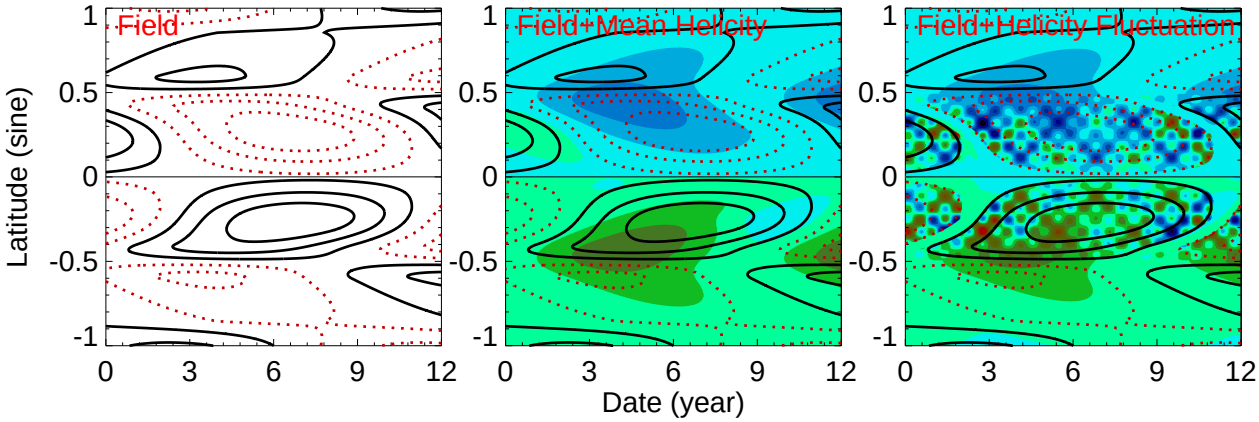


**Figure 8.** The schematics on the relationship between the magnetic field and injective helicity with the solar cycle. Left: large scale magnetic field with the solar cycle. The solid (dotted) lines show the positive (negative) polarity. Middle: the large-scale magnetic field overlapped by the mean values of large scale injective magnetic helicity, the blue is negative and green is positive sign. Right: the large-scale magnetic field overlapped by the small-scale dispersed helicity from fluctuating magnetic fields to morphologically compare Figs 1b and c.

components (such as Zeldovich et al. 1983)

$$B = \sum_m b_m \cdot \exp(\gamma_m t + i\kappa_m \theta + \varphi_m)$$
$$A = \sum_n a_n \cdot \exp(\gamma_n t + i\kappa_n \theta + \varphi_n), \quad (8)$$

where $B$ and $A$ are composed of different time and spatial scale components $b_m$ and $a_n$, respectively.

As the phase difference between $\varphi_m$ and $\varphi_n$ and the interaction of the different temporal and spatial scales of magnetic fields and their potentials are negligible (i.e. $\varphi_m = \varphi_n$, $\gamma_m = \gamma_n$ and $\kappa_m = \kappa_n$), the magnetic helicity density can be written in the form (see Xu et al. 2009; Popova & Nefedov 2010)

$$H_{\rm m} = A \cdot B = \sum_n a_n b_n \cdot \exp(2\gamma_n t + 2i\kappa_n \theta) + ...., \quad (9)$$

where the magnetic helicity consists with different temporal and spatial scale helicity components. Thus the flux change of magnetic helicity can be written in the form

$$\frac{\partial H_{\rm m}}{\partial t} = \sum_n a_n b_n 2\gamma_n \cdot \exp(2\gamma_n t + 2i\kappa_n \theta) + .... \quad (10)$$

and it can be written, after some calculation (Zhang 2012) in the form

$$\frac{\partial H_{\rm m}}{\partial t} = \sum_n 2\gamma_n \left(\frac{\alpha_n}{\kappa_n |D_n|}\right)^{1/2} \exp\left(2\gamma_n t + 2i\kappa_n \theta + \frac{i\pi}{4}\right). \quad (11)$$

Figure 8 shows the schematics of the distribution of magnetic field and injective helicity with solar cycles. The mean large scale magnetic helicity tends to show a negative (positive) sign in the northern (southern) hemisphere, while the reverse of large-scale magnetic helicity in the decaying phase of the solar cycles was analytically demonstrated by (Xu et al. 2009; Popova & Nefedov 2010; Zhang 2012). For analyzing in more detail, the small-scale fluctuating components of magnetic helicity have been overlaid with the large-scale ones. It is roughly consistent with the distribution of the observed injective helicity in the form of butterfly diagrams in Fig. 1 and consistent with the butterdiagram of the observed current helicity of active regions by Zhang et al. (2010) (i.e. $dH_{\rm m}/dt \sim a_n b_n$ in equation (10)). This also probably can be used to reflect the formation and transformation between the large scale toroidal and poloidal fields inside of the Sun.

## 5 DISCUSSIONS AND CONCLUSIONS

In this paper, the collective effect of injective magnetic helicity during solar cycles and individual samples of magnetic helicity with the evolution of magnetic field in active regions have been presented. To analyze the helicity formation in the solar subsurface, the collective effect of the injective magnetic helicity with the magnetic fields of solar cycle 24 has been presented based on the analysis of a series of magnetic synoptic charts. The sign distribution of injective magnetic helicity shows the dispersed form contributed from individual local regions (such as active regions) with solar cycles, and it is hard to find the helicity in the polar regions, due to the eruption of magnetic field from the sub-atmosphere into the interplanetary space.

For presenting the evolution of magnetic helicity with solar cycles, a morphological analysis of the helicity patterns with butterfly diagram has been proposed, which are composed of different scale fluctuating components, such as characterized by solar active regions. This probably reflects the complex process of twisted magnetic field inside of the convection due to the interaction the Coriolis force and meridional circulation on the formation of magnetic lines of force.

We have analyzed the evolution of the magnetic helicity in active region NOAA 12673 and the relationship with the sequence of solar active regions NOAA 12670, 12682, 12685 in different solar Carrington rotation cycles. The reversal magnetic helicity occurs in the solar surface with emergence of newly emergence of magnetic flux in the active region. This probably reflects the interaction the existed magnetic field of the active regions with the new magnetic flux formed in the deep convection zone with the injection of the magnetic helicity, with the exchange of the local poloidal and toroidal fields.

We have formally tried to reproduce the helicity distribution in the solar surface in Fig. 8 by means of equation (10). There is still the related fundamental question on the generation of magnetic fields of the different scales with velocity fields in the deep convection zone, while the strong magnetic flux loops are mainly characterized by the solar active regions.

Although the calculation of the injective magnetic helicity flux with the synoptic magnetic charts has been calculated based on the corresponding temporal and spatial scales of magnetic fields, the detailed analysis of the contribution of the evolution of the magnetic field with the solar cycle still needs to be based on the observed full disk magnetograms. It is noticed that as the different temporal and spatial scale observed solar magnetic fields have been used in the analysis, the statistical results probably has some difference, while the trend probably is the same.

## ACKNOWLEDGEMENTS

The authors would like to thank the staff at the *Solar Dynamics Observatory* (SDO) for providing the observational data. The authors would like to thank Dr. V. Pipin for useful discussions. This study is supported by grants from the National Natural Science Foundation (NNSF) of China under the project grant 11673033, 11427803, 11427901, 11703042, 11911530089 and other grant at Huairou Solar Observing Station, National Astronomical Observatories, Chinese Academy of Sciences. This work was supported in part through the Swedish Research Council, grant 2019-04234.

## REFERENCES

Bao, S.D., Zhang, H.Q., Ai, G.X., and Zhang, M.: 1999, *Astron. Astrophys. Suppl.* **139**, 311.
Bao S. D., Ai G. X., Zhang H. Q., 2000, J. Astrophys. Astron., **21**, 303
Berger, M. A. & Field, G. B., 1984, *J. Fluid Mech.*, **147**, 133
Brandenburg, A., & Subramanian, K. 2005, Solar Physics, **417**, 1
Chae J., 2001, Astrophys. J., **560**, L95
Choudhuri, A. R., Chatterjee, P., & Nandy, D. 2004, Astrophys. J., **615**, L57
Démoulin, P. & Berger, M. A. 2003, Solar Physics, **215**, 203
Ding, Y. J., Hong, Q. F., Wang, H. Z., 1987, Solar Physics, **107**, 221
Getling, A. V., 2019, Astrophys. J., **878**, 127
Hagino, M. & Sakurai, T., 2005, Publ. Astron. Soc. Japan., **57**, 481
Hale, G. E., 1908, Astrophys. J., **28**, 315
Kleeorin, N. I., & Ruzmaikin, A. A. 1982, Magnetohydrodynamics, **18**, 116
Kleeorin, N.; Rogachevskii, I.; Ruzmaikin, A., 1995, Astron. Astrophys., **297**, 159
Kleeorin, N., & Rogachevskii, I. 1999, Phys. Rev.E, **59**, 6724
Kleeorin N., Kuzanyan K., Moss D., Rogachevskii I., Sokoloff D., & Zhang H. 2003, Astron. Astrophys., **409**, 1097
Liu, J. H. & Zhang, H. Q., 2006, Solar Physics, **234**, 21
Liu, Y. & Schuck, P. W. 2012, Astrophys. J., **761**, L105
Longcope, D. W., Fisher, G. H. & Pevtsov, A. A., 1998, Astrophys. J., **507**, L417
Moffatt, H.K. 1978, *Magnetic field generation in electrically conducting fluids*, Cambridge University Press, Cambridge
Parker, E. 1955, Astrophys. J., **122**, 293
Parker, E. N. 1979, Cosmical Magnetic Fields - Their Origin and Their Activity, Oxford University Press
Pipin, V. V., Zhang, H., Sokoloff, D. D., Kuzanyan, K. M., & Gao, Y., 2013, Mon. Not. R. Astron. Soc., **435**, 2581
Pipin, V. V., Pevtsov, A.A., Liu, Y., Kosovichev, A. G. 2019, Astrophys. J., **877**, L36
Popova E. P. and Nefedov S. N., 2010, Moscow University Physics Bulletin, **65**, 2, 86
Pouquet, A., Frisch, U., & Léorat, J. 1975, J. Fluid Mech., **68**, 769
Romano, P., Elmhamdi, A., & Kordi, A. S., 2019, Solar Physics, **294**, 4
Schuck, P. W. 2008, Astrophys. J., **683**, 1134
Seehafer N., 1990, Solar Physics, **125**, 219
Steenbeck, M., Krause, F. & RÄd'dler, K. H., 1966, ZNatA, 21, 369
Sun, X., & Norton, A., 2017, RNAAS, **1a**, 24.
Taylor, J. B., 1986, RvMP, **58**, 741
Wang, Y. M., Nash, A. G., and Sheeley, N. R. Astrophys. J., 1989a, **347**, 529
Woltjer, L. 1958a, Proc. Natl Acad. Sci. USA, **44**, 480
Woltjer L., 1958b, Proc. Nat. Acad. Sci., USA, **44**, 833
Xu, H., Gao, Y., E.P. Popova, S.N., Nefedov, Zhang, H. and D.D. Sokoloff, 2009, *Astron. Reports*, **53**, 160
Xu, H., Stepanov, R., Kuzanyan, K., Sokoloff, D., Zhang, H., & Gao, Y. 2015, Mon. Not. R. Astron. Soc., **454**, 1921
Yang, S. B. & Zhang, H., 2012, Astrophys. J., **758**, 61
Yang, X, Zhang, H., Gao, Y., Guo, J. and Lin, G., 2012, Solar Physics, **280**, 165
Yang, S. H., Zhang, J., Zhu, X. & Song, Q., 2017, Astrophys. J., **849**, L21.

Zeldovich, Ia. B., Ruzmaikin, A. A. & Sokoloff, D. D., 1983, Magnetic fields in astrophysics, Gordon and Breach Science Publishers
Zhang, H., 2000, Solar Physics, **197**, 235
Zhang, H., 2001, Mon. Not. R. Astron. Soc., **326**, 57
Zhang, H., 2012, Mon. Not. R. Astron. Soc., **419**, 799, Erratum: Mon. Not. R. Astron. Soc., **493**, 1317
Zhang, H., 2016, Solar Physics, **291**, 3501.
Zhang, H., 2019, SCIENCE CHINA, Physics, Mechanics & Astronomy, 62 No. 9: 999601
Zhang, H., Labonte, B., Li, J., and Sakurai, T., 2003, Solar Physics, **213**, 87.
Zhang, Y., Liu, J. H., and Zhang, H. Q., 2008, Solar Physics, **247**, 39
Zhang, H., Sakurai, T., Pevtsov, A., Gao, Y., Xu, H., Sokoloff, D., Kuzanyan, K. 2010, Mon. Not. R. Astron. Soc., **402**, L30
Zhang, H., Moss, D., Kleeorin, N., Kuzanyan, K., Rogachevskii, I., Sokoloff, D., Gao, Y. and Xu, H., 2012, Astrophys. J., **751**, 47
Zhang, H. & Yang, S., 2013, Astrophys. J., **763**, 105
Zhang, H., Brandenburg A. and Sokoloff D., 2016, Astrophys. J., **819**, 146
Zhao, J., Bogart, R. S., Kosovichev, A. G., Duvall, T. L., Jr., & Hartlep, T., 2013, Astrophys. J., **774**, L29

This paper has been typeset from a TEX/LATEX file prepared by the author.